LETTER

doi:10.1038/nature25021

Acoustic reporter genes for noninvasive imaging of microorganisms in mammalian hosts

Raymond W. Bourdeau[1], Audrey Lee-Gosselin[1], Anupama Lakshmanan[2], Arash Farhadi[2], Sripriya Ravindra Kumar[2], Suchita P. Nety[1] & Mikhail G. Shapiro[1]

The mammalian microbiome has many important roles in health and disease[1,2], and genetic engineering is enabling the development of microbial therapeutics and diagnostics[3–7]. A key determinant of the activity of both natural and engineered microorganisms *in vivo* is their location within the host organism[8,9]. However, existing methods for imaging cellular location and function, primarily based on optical reporter genes, have limited deep tissue performance owing to light scattering or require radioactive tracers[10–12]. Here we introduce acoustic reporter genes, which are genetic constructs that allow bacterial gene expression to be visualized *in vivo* using ultrasound, a widely available inexpensive technique with deep tissue penetration and high spatial resolution[13–15]. These constructs are based on gas vesicles, a unique class of gas-filled protein nanostructures that are expressed primarily in water-dwelling photosynthetic organisms as a means to regulate buoyancy[16,17]. Heterologous expression of engineered gene clusters encoding gas vesicles allows *Escherichia coli* and *Salmonella typhimurium* to be imaged noninvasively at volumetric densities below 0.01% with a resolution of less than 100 μm. We demonstrate the imaging of engineered cells *in vivo* in proof-of-concept models of gastrointestinal and tumour localization, and develop acoustically distinct reporters that enable multiplexed imaging of cellular populations. This technology equips microbial cells with a means to be visualized deep inside mammalian hosts, facilitating the study of the mammalian microbiome and the development of diagnostic and therapeutic cellular agents.

Gas vesicles comprise all-protein shells with sizes of approximately 200 nm that enclose hollow interiors, and allow dissolved gases to permeate freely in and out while excluding water[16]. We recently discovered the ability of these proteins to scatter sound waves and thereby produce ultrasound contrast[18]. However, the ability of the multi-gene clusters encoding gas vesicles to serve as reporter genes in heterologous species has not been demonstrated. Gas vesicles are encoded in their native bacterial or archaeal hosts by operons of 8–14 genes, which include the primary structural protein GvpA, the optional external scaffolding protein GvpC, and several secondary proteins that function as essential minor constituents or chaperones[17]. As a starting point for developing acoustic reporter genes (ARGs), we chose a compact *E. coli*-compatible gas vesicle gene cluster from *Bacillus megaterium*[19] (Fig. 1a; top left). Although cells containing this construct were able to produce small, bicone-shaped gas vesicles (Fig. 1b, c; left), its expression did not result in bacteria that were detectable by ultrasound (Fig. 1d; left), most probably because the small gas vesicles produced from this construct have weak acoustic scattering. At the same time, transforming *E. coli* with a gas vesicle gene cluster derived from the cyanobacterium *Anabaena flos-aquae*, the gas vesicles of which are highly echogenic[18,20], did not result in gas vesicle expression. Given the high sequence homology of GvpA between organisms (Extended Data Fig. 1), we hypothesized that a combination of the structural *gvpA* genes from *A. flos-aquae* with the accessory genes *gvpR–gvpU* from *B. megaterium* (Fig. 1a; middle) would result in the formation of gas vesicles with characteristics favourable for ultrasound imaging. Indeed, expression of this engineered gene cluster resulted in *E. coli* containing gas vesicles with substantially larger dimensions compared to the *B. megaterium* operon, and these nanostructures appeared to occupy a greater fraction of intracellular volume (Fig. 1b, c; middle). Notably, these cells produced robust ultrasound contrast compared to green fluorescent protein (GFP) controls (Fig. 1d; middle). Further engineering comprising the addition of a gene encoding the *A. flos-aquae* scaffolding protein GvpC (Fig. 1a; right) resulted in wider and more elongated gas vesicles that more closely resembled those native to *A. flos-aquae*[18] (Fig. 1b, c; right), and generated stronger ultrasound contrast (Fig. 1d; right). We refer to this optimized genetically engineered construct as acoustic reporter gene 1 or *arg1*.

To confirm that the ultrasound signal from *arg1*-expressing cells is due to the presence of gas vesicles, we applied acoustic pulses with amplitudes above the critical collapse pressure of the gas vesicles[20]. In purified samples, this resulted in the immediate collapse of these protein nanostructures and dissolution of their gas contents, eliminating ultrasound contrast[18,20]. As expected, the application of high-pressure pulses made cells expressing *arg1* invisible to ultrasound (Fig. 1d). The ability of ARG-based contrast to be erased *in situ* is used throughout this study to confirm the source of acoustic signals and subtract background.

arg1 expression resulted in gas vesicle contents of 9.4 ± 0.4 mg g^{-1} *E. coli* ($n = 3$, mean ± s.e.m.), corresponding to approximately 100 gas vesicles per cell. These nanostructures occupy roughly 10% of the intracellular space. Acoustically silent cells expressing the *B. megaterium* gene cluster produced a similar quantity of gas vesicle proteins (9.7 ± 1.5 mg g^{-1}, $n = 3$), underscoring the importance of genetic engineering in producing intracellular nanostructures with the appropriate size and shape to be detected by ultrasound. A fraction of *arg1*-expressing cells was buoyant in aqueous medium (Extended Data Fig. 2a, b), suggesting that gas vesicles occupy more than 10% of their volume. However, the expected buoyant force on these cells, even at much higher expression levels, is weak compared to other forces such as flagellar thrust (Supplementary Table 1).

To determine the detection limit of ARG-expressing cells, we imaged a concentration series of *E. coli* transformed with *arg1* (Fig. 2a). Cells at concentrations as low as 5×10^7 cells ml^{-1} produced a detectable signal (Fig. 2a, b). This equates to a roughly 0.005% volume fraction, or approximately 100 cells per voxel based on cubic voxel dimensions of 100 μm. This sensitivity should be sufficient for many *in vivo* scenarios[21]. Furthermore, bacteria enriched for buoyancy before imaging provide a 2.4-fold higher signal (Extended Data Fig. 2c, d), suggesting that sensitivity could be improved further by optimizing ARG expression.

To test whether ARGs could provide a read-out of state-dependent genetic pathways, we placed *arg1* under the control of a promoter

[1]Division of Chemistry and Chemical Engineering, California Institute of Technology, Pasadena, California 91125, USA. [2]Division of Biology and Biological Engineering, California Institute of Technology, Pasadena, California 91125, USA.

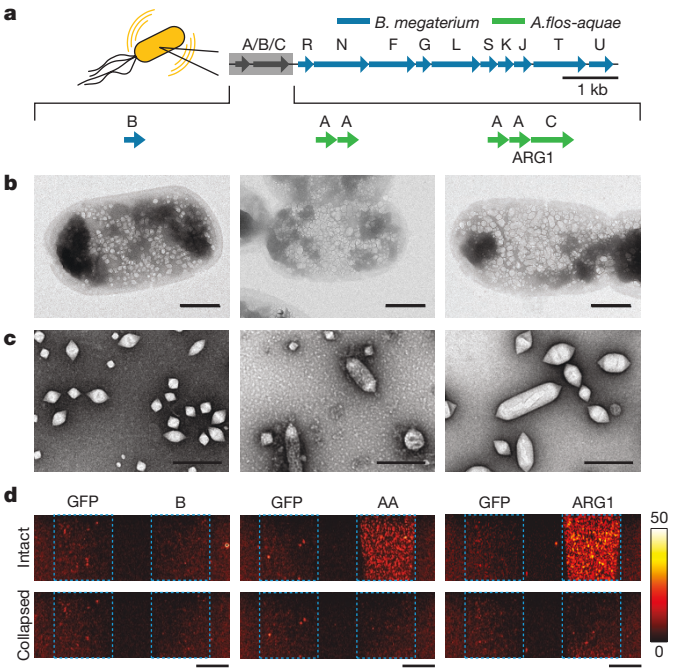

Figure 1 | Genetic engineering of acoustic reporter genes. **a**, Organization of acoustic reporter gene clusters; the region highlighted in grey was varied. Panels **b**–**d** are organized in columns that correspond to each of the variant constructs. **b**, TEM images of representative *E. coli* cells expressing each construct. **c**, TEM images of gas vesicles isolated from *E. coli* expressing each construct. **d**, Ultrasound images of agarose phantoms containing *E. coli* expressing each construct or GFP. The cell concentration is 10^9 cells ml^{-1}. Images in the bottom panels were acquired after acoustic collapse. Dotted blue outlines indicate the location of each specimen. Colour bar represents linear signal intensity. Scale bars, 500 nm (**b**), 250 nm (**c**) and 2 mm (**d**). All imaging experiments were repeated three times with similar results.

regulated by the chemical inducer isopropyl-β-D-thiogalactoside (IPTG). Ultrasound signals from *E. coli* expressing ARGs in this configuration followed the expected dose–response curve of IPTG-controlled expression (Fig. 2c, d), confirming their ability to serve as the output signal for engineered genetic circuits. Significant ultrasound contrast could be observed 4 h after IPTG induction ($P = 0.01$, $n = 4$),

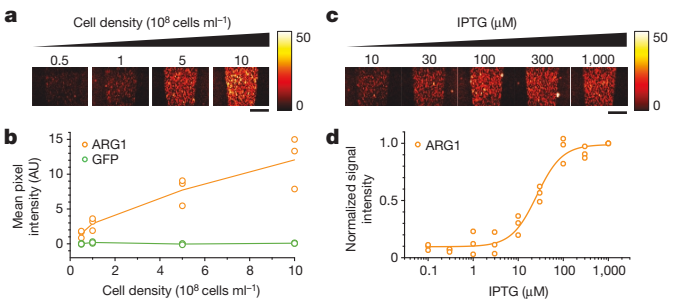

Figure 2 | Imaging dilute bacterial populations and dynamically regulated gene expression. **a**, Ultrasound images of *arg1*-expressing *E. coli* at various cellular concentrations, before and after acoustic collapse. **b**, Mean ultrasound contrast from *E. coli* expressing *arg1* and GFP at various cell densities. Data are from three biological replicates, lines indicate the mean. AU, arbitrary units. **c**, Ultrasound images of *E. coli* expressing *arg1* after induction with various concentrations of IPTG. Cell concentration was 5×10^8 cells ml^{-1}. **d**, Normalized ultrasound contrast as a function of IPTG concentration. Data are from three biological replicates, line shows a fit of the data with the Hill equation to facilitate visualization. Each imaging experiment was repeated three times with similar results. Scale bars, 2 mm.

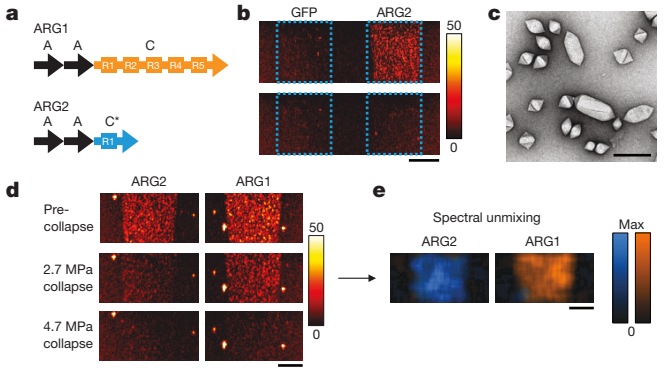

Figure 3 | Multiplexed imaging of genetically engineered reporter variants. **a**, Diagram of the *gvpA* and *gvpC* sequences included in the *arg1* and *arg2* gene clusters. **b**, Ultrasound images of a gel phantom containing *E. coli* expressing GFP or *arg2* (10^9 cells ml^{-1}). Dotted blue outlines indicate the location of each specimen. **c**, TEM images of isolated *arg2* gas vesicles. **d**, Ultrasound images of gel phantoms containing *arg1* or *arg2* before collapse, after collapse at 2.7 MPa and after collapse at 4.7 MPa (10^9 cells ml^{-1}). **e**, Overlay of the blue and orange maps from spectral unmixing of *arg2* and *arg1*, based on the series of images in **d**. Scale bars, 2 mm (**b**, **d**, **e**) and 250 nm (**c**). Each imaging experiment was repeated three times with similar results.

and continued to increase during the 22-h culturing period (Extended Data Fig. 3).

To determine whether the expression of ARGs has any deleterious effect on host cells, we measured the growth curves of *E. coli* expressing *arg1* or GFP. After induction, cells expressing both constructs continued to divide and reached similar saturation densities (Extended Data Fig. 4a). For both *arg1* and GFP, the final density was lower than in uninduced controls, as expected from the metabolic demand of protein expression[22]. We also assessed the viability of ARG-expressing cells after ultrasound imaging and acoustic collapse. Transmission electron microscopy (TEM) images of cells acquired before and after exposure to collapsing acoustic pulses show that gas vesicles can be eliminated without any obvious cellular damage (Extended Data Fig. 4b). To examine the effect of ultrasound exposure on cell growth, we cultured *E. coli* expressing *arg1* as colonies on solid medium and applied acoustic collapse pulses to half of the agar plate. The collapse of gas vesicles in insonated cells was confirmed by a decrease in optical scattering (Extended Data Fig. 4c, d). After incubation for an additional 20 h, no significant difference was observed in the diameter of the insonated colonies compared to un-insonated controls, indicating that ultrasound exposure does not affect cell viability (Extended Data Fig. 4e). Notably, insonated colonies re-expressed gas vesicles during this period, as indicated by the restoration of pressure-sensitive light scattering (Extended Data Fig. 4e, f).

It is often informative to image more than one population of cells simultaneously, as done optically using spectrally distinct fluorescent proteins. Analogous acoustic multiplexing can be performed using genetic variants of gas vesicles that collapse at different pressures using multiple images acquired during sequential application of increasing pressure pulses[20] (Supplementary Note 1). To explore whether this could be done with ARGs, we constructed a new version of the ARG-expressing gene cluster containing a modified version of *A. flos-aquae gvpC*. Deletion or truncation of this outer scaffolding protein results in gas vesicles with lower collapse pressures[23], allowing the production of nanostructures that are distinguishable from each other under ultrasound[20]. Using this approach, we modified our gene cluster by truncating GvpC to retain only one of its five repeating α-helical domains (Fig. 3a). *E. coli* expressing the resulting gene cluster, which we refer to as *arg2*, showed robust production of gas vesicles and ultrasound contrast, similar to *arg1* (Fig. 3b, c and Extended Data Fig. 5a–c). Consistent with our design, gas vesicles purified from *arg2*-expressing *E. coli* had a lower critical hydrostatic collapse pressure

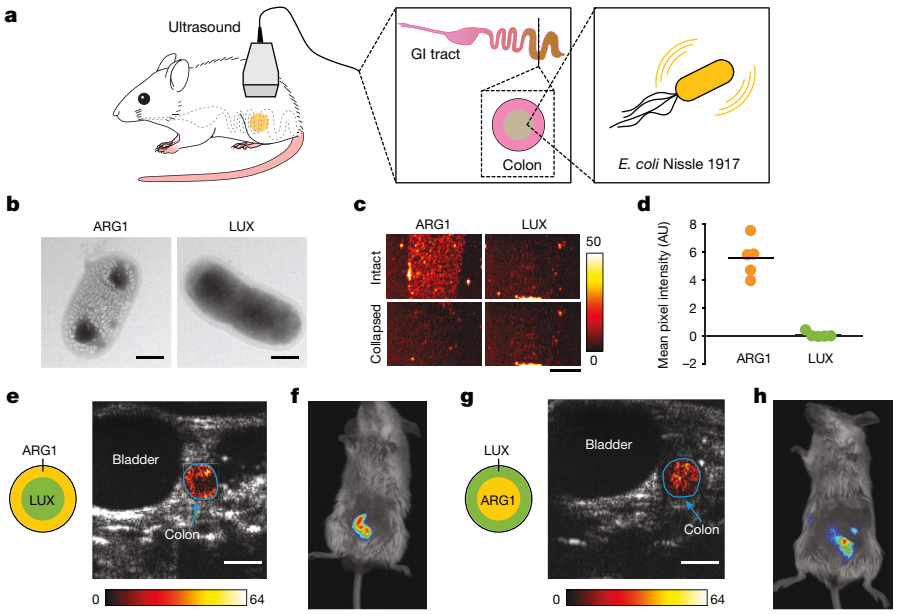

Figure 4 | Ultrasound imaging of bacteria in the gastrointestinal tract. **a**, Diagram of gastrointestinal (GI) imaging experiment. **b**, Representative TEM images of whole ECN cells expressing *arg1* or the *lux* operon. Images were acquired from three biologically independent samples for *arg1* and one for *lux* (approximately 35 cells imaged in each sample) with similar results. **c**, Ultrasound images of a gel phantom containing ECN expressing *arg1* or the *lux* operon. Experiment repeated five times with similar results. **d**, Mean collapse-sensitive ultrasound signal in phantoms containing ECN cells expressing *arg1* or *lux*. Line represents mean. ($P = 0.0007$ using a two-sided heteroscedastic *t*-test, $n = 5$). Cell concentration in **c**–**d** was 10^9 cells ml^{-1}. **e**, Transverse ultrasound image of a mouse whose colon contains ECN expressing *arg1* proximal to the colon wall, and ECN expressing *lux* at the centre of the lumen. **f**, Luminescence image of mouse with the same arrangement of colonic bacteria. **g**, **h**, As in **e** and **f**, but with ECN expressing *arg1* at the centre of the lumen and ECN expressing *lux* at the periphery. Cells are loaded at a final concentration of 10^9 cells ml^{-1}. In **e** and **g**, a difference heat map of ultrasound contrast within the colon region of interest before and after acoustic collapse is overlaid on a greyscale anatomical image. In **f** and **h**, a thresholded luminescence map is overlaid on a bright-field image of the mouse. Scale bars, 500 nm (**b**), 2 mm (**c**) and 2.5 mm (**e**, **g**). *In vivo* imaging experiments were repeated three times with similar results.

than nanostructures formed by cells expressing *arg1* (Extended Data Fig. 5d), and cellular *arg2* contrast was erasable at lower acoustic pressures (Extended Data Fig. 5e). The distinct collapse spectra of the two variants (Extended Data Fig. 5f) allowed *E. coli* expressing *arg1* and *arg2* to be imaged in multiplex using pressure spectrum unmixing (Fig. 3d, e).

After establishing the core capabilities of ARGs *in vitro*, we set out to demonstrate their detectability *in vivo* by imaging ARG-expressing cells in biologically relevant anatomical contexts. One important target for *in vivo* microbial imaging is the mammalian gastrointestinal tract, given the effect of the gut microbiome on the host's health[1,8,9] and the development of gastrointestinal-targeted microbial therapeutics[4,24]. Owing to its location deep inside the body, the gastrointestinal tract is difficult to image using optical techniques. To establish a proof of concept for ultrasonic imaging of microorganisms in this context, we expressed ARGs in a probiotic bacterial strain and assessed the ability of ultrasound to localize this bacterium inside the colon (Fig. 4a) in comparison with bioluminescent imaging. The *E. coli* strain Nissle 1917 (ECN) is a probiotic microorganism capable of colonizing the mammalian gastrointestinal tract[25]. ECN has been used clinically in humans for 100 years to treat enteric infection and inflammatory bowel conditions[25], and is a common chassis for therapeutic synthetic biology[3,5,6,26]. ECN cells transformed with a plasmid expressing *arg1* produced abundant gas vesicles (Fig. 4b) and ultrasound contrast (Fig. 4c, d). For comparison, we transformed ECN cells with the luminescence operon *luxABCDE* (*lux*), which has previously been used to visualize gene expression in microbial populations *in vivo* using bioluminescent imaging[3,6,27]. *lux*-expressing ECN cells produced no ultrasound contrast (Fig. 4c, d).

To establish a proof of concept for ultrasound imaging of ARG-expressing bacteria within the gastrointestinal tract, and to compare the result with bioluminescent imaging, we introduced ECN cells expressing *arg1* or *lux* into the colons of anaesthetized mice. To assess the ability of each modality to resolve the spatial distribution of bacteria within the colon, we injected the *arg1* and *lux* cells into the centre or periphery of the colonic lumen (Fig. 4e–h). Ultrasound images clearly revealed the localization of ARG-expressing ECN cells in the appropriate region of the colon (Fig. 4e, g) at concentrations of 10^9 cells ml^{-1}, which is within the range of certain commensal and therapeutic scenarios, and below the density reached by ECN in gnotobiotic models[21,25]. By contrast, bioluminescent images showed only that the bacteria are present somewhere in the mouse abdomen (Fig. 4f, h). To facilitate visualization of ARG-specific signals, our ultrasound image analysis used background subtraction after gas vesicle collapse, with the resulting contrast overlaid on greyscale anatomical images to show the location of the bacteria within the context of other internal organs. Alternatively, ARG-expressing cells can also be seen in the colon in raw ultrasound images (Extended Data Fig. 6). Contrast from colon-localized *E. coli* was consistent across mice (Extended Data Fig. 7). These results establish the ability of ARGs to make genetically-labelled microorganisms visible noninvasively in deep tissue, and demonstrate the advantage of ultrasound relative to optical imaging in terms of spatial localization within deep organs.

Some degree of burden is expected to accompany heterologous protein expression[28,29]. To assess the burden on ECN cells presented by *arg1*, we characterized their growth, viability, maintenance of reporter expression and release of microcins. We observed that *arg1* expression is generally well tolerated, with some scope for optimization (Extended Data Fig. 8 and Supplementary Note 2).

In addition to the gastrointestinal tract, another emerging application of engineered microorganisms is in antitumour therapies and diagnostics[3,6,30]. To test whether such microorganisms could be imaged with ultrasound, and assess whether ARGs could be generalized to additional species besides *E. coli*, we adapted the genetic construct encoding *arg1* for expression in the attenuated, tumour-homing *S. typhimurium* strain ELH1301 (refs 16, 30), and showed that we could

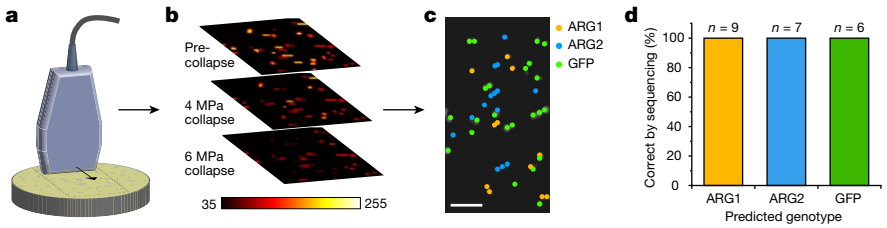

Figure 5 | High-throughput screening of acoustic phenotypes. **a**, Illustration of acoustic colony screening. **b**, Colony ultrasound images of a mixed population of *E. coli* colonies expressing *arg1*, *arg2*, and GFP. Images were acquired before collapse and after collapse at peak acoustic pressures of 4 and 6 MPa. This imaging experiment was performed once; each colony was treated as a biological replicate. **c**, Predicted genotypes of each colony based on the acoustic phenotype seen in the images in **b**. Scale bar, 10 mm. **d**, Confirmation of predicted genotypes by colony picking and sequencing. *n*, number of sequenced colonies of each type.

image these cells after injection into tumours (Extended Data Fig. 9 and Supplementary Note 3).

Finally, to facilitate future genetic engineering of ARGs, we assessed the amenability of these constructs to high-throughput screening. In fluorescent protein engineering, directed evolution has served as an effective approach to identify variants with new spectral and biochemical properties[31,32], often using mutant bacterial colonies as a convenient platform for high-throughput screening[32]. To determine whether a similar approach could be used with ARGs, we developed a method to scan bacterial colonies with ultrasound (Fig. 5a). In this method, colonies are immobilized on agar plates with an over-layer of agarose, then scanned with an ultrasound transducer translated by a computer-controlled robot. This results in a series of transverse images that can be reconstructed to form an in-plane image of the plate (Fig. 5b). We used this technique to image a mixed plate of *E. coli* transformed with *arg1*, *arg2* or GFP. Serial acoustic collapse imaging (Fig. 5b) revealed three distinct colony populations (Fig. 5c and Extended Data Fig. 10), allowing the genotypes to be distinguished from each other with 100% accuracy (Fig. 5d). This result suggests that colony screening can discriminate acoustic phenotypes with sufficient accuracy to serve as a high-throughput assay for acoustic protein engineering.

Our study establishes engineered gas vesicle gene clusters as reporter genes for ultrasound, giving this widely used noninvasive imaging modality the ability to visualize genetically modified bacteria inside living animals. Future work will build on the *in vitro* and *in vivo* proofs of concept presented in this study to answer scientific and translational questions. This research will benefit from the development of ultrasound techniques to detect ARG signals and distinguish them from background (Supplementary Note 4), further genetic engineering to optimize the stability and host burden of ARG constructs, and expression of these reporters in a broader range of microbial species (Supplementary Note 5). In addition, it is ultimately desirable to express ARGs in mammalian cells.

We anticipate that the ARGs presented in this work are a starting point for future engineering of ultrasound reporter genes. Since their initial discovery as optical reporters, fluorescent proteins have been engineered, evolved and used in thousands of unforeseen optical imaging applications. Our findings that genetic engineering can be used to generate ARGs with distinct acoustic properties and that ARGs are amenable to colony-based high-throughput screening suggest that a similar trajectory may be available for this new technology.

Online Content Methods, along with any additional Extended Data display items and Source Data, are available in the online version of the paper; references unique to these sections appear only in the online paper.

Received 21 December 2016; accepted 9 November 2017.

1. Round, J. L. & Mazmanian, S. K. The gut microbiota shapes intestinal immune responses during health and disease. *Nat. Rev. Immunol.* **9,** 313–323 (2009).
2. Wang, Y. & Kasper, L. H. The role of microbiome in central nervous system disorders. *Brain Behav. Immun.* **38,** 1–12 (2014).
3. Danino, T. *et al.* Programmable probiotics for detection of cancer in urine. *Sci. Transl. Med.* **7,** 289ra284 (2015).
4. Steidler, L. *et al.* Treatment of murine colitis by *Lactococcus lactis* secreting interleukin-10. *Science* **289,** 1352–1355 (2000).
5. Claesen, J. & Fischbach, M. A. Synthetic microbes as drug delivery systems. *ACS Synth. Biol.* **4,** 358–364 (2015).
6. Din, M. O. *et al.* Synchronized cycles of bacterial lysis for *in vivo* delivery. *Nature* **536,** 81–85 (2016).
7. Riglar, D. T. *et al.* Engineered bacteria can function in the mammalian gut long-term as live diagnostics of inflammation. *Nat. Biotechnol.* **35,** 653–658 (2017).
8. Donaldson, G. P., Lee, S. M. & Mazmanian, S. K. Gut biogeography of the bacterial microbiota. *Nat. Rev. Microbiol.* **14,** 20–32 (2016).
9. Derrien, M. & van Hylckama Vlieg, J. E. Fate, activity, and impact of ingested bacteria within the human gut microbiota. *Trends Microbiol.* **23,** 354–366 (2015).
10. Foucault, M.-L., Thomas, L., Goussard, S., Branchini, B. R. & Grillot-Courvalin, C. *In vivo* bioluminescence imaging for the study of intestinal colonization by *Escherichia coli* in mice. *Appl. Environ. Microbiol.* **76,** 264–274 (2010).
11. Daniel, C., Poiret, S., Dennin, V., Boutillier, D. & Pot, B. Bioluminescence imaging study of spatial and temporal persistence of *Lactobacillus plantarum* and *Lactococcus lactis* in living mice. *Appl. Environ. Microbiol.* **79,** 1086–1094 (2013).
12. Chu, J. *et al.* A bright cyan–excitable orange fluorescent protein facilitates dual-emission microscopy and enhances bioluminescence imaging *in vivo*. *Nat. Biotechnol.* **34,** 760–767 (2016).
13. Smith-Bindman, R. *et al.* Use of diagnostic imaging studies and associated radiation exposure for patients enrolled in large integrated health care systems, 1996-2010. *J. Am. Med. Assoc.* **307,** 2400–2409 (2012).
14. Foster, F. S. *et al.* Principles and applications of ultrasound backscatter microscopy. *IEEE Trans. Ultrason. Ferroelectr. Freq. Control* **40,** 608–617 (1993).
15. Errico, C. *et al.* Ultrafast ultrasound localization microscopy for deep super-resolution vascular imaging. *Nature* **527,** 499–502 (2015).
16. Walsby, A. E. Gas vesicles. *Microbiol. Rev.* **58,** 94–144 (1994).
17. Pfeifer, F. Distribution, formation and regulation of gas vesicles. *Nat. Rev. Microbiol.* **10,** 705–715 (2012).
18. Shapiro, M. G. *et al.* Biogenic gas nanostructures as ultrasonic molecular reporters. *Nat. Nanotechnol.* **9,** 311–316 (2014).
19. Li, N. & Cannon, M. C. Gas vesicle genes identified in *Bacillus megaterium* and functional expression in *Escherichia coli*. *J. Bacteriol.* **180,** 2450–2458 (1998).
20. Lakshmanan, A. *et al.* Molecular engineering of acoustic protein nanostructures. *ACS Nano* **10,** 7314–7322 (2016).
21. Gorbach, S. L. in *Medical Microbiology* 4th edn (ed. Baron, S.) Ch. 95 (Univ. Texas Medical Branch, 1996).
22. Klumpp, S. & Hwa, T. Bacterial growth: global effects on gene expression, growth feedback and proteome partition. *Curr. Opin. Biotechnol.* **28,** 96–102 (2014).
23. Hayes, P. K., Buchholz, B. & Walsby, A. E. Gas vesicles are strengthened by the outer-surface protein, GvpC. *Arch. Microbiol.* **157,** 229–234 (1992).
24. Daniel, C., Roussel, Y., Kleerebezem, M. & Pot, B. Recombinant lactic acid bacteria as mucosal biotherapeutic agents. *Trends Biotechnol.* **29,** 499–508 (2011).
25. Sonnenborn, U. & Schulze, J. The non-pathogenic *Escherichia coli* strain Nissle 1917—features of a versatile probiotic. *Microb. Ecol. Health Dis.* **21,** 122–158 (2009).
26. Chen, Z. *et al.* Incorporation of therapeutically modified bacteria into gut microbiota inhibits obesity. *J. Clin. Invest.* **124,** 3391–3406 (2014).
27. Francis, K. P. *et al.* Monitoring bioluminescent *Staphylococcus aureus* infections in living mice using a novel *luxABCDE* construct. *Infect. Immun.* **68,** 3594–3600 (2000).
28. Borkowski, O., Ceroni, F., Stan, G.-B. & Ellis, T. Overloaded and stressed: whole-cell considerations for bacterial synthetic biology. *Curr. Opin. Microbiol.* **33,** 123–130 (2016).
29. Sleight, S. C. & Sauro, H. M. Visualization of evolutionary stability dynamics and competitive fitness of *Escherichia coli* engineered with randomized multigene circuits. *ACS Synth. Biol.* **2,** 519–528 (2013).
30. Danino, T., Lo, J., Prindle, A., Hasty, J. & Bhatia, S. N. *In vivo* gene expression dynamics of tumor-targeted bacteria. *ACS Synth. Biol.* **1,** 465–470 (2012).
31. Romero, P. A. & Arnold, F. H. Exploring protein fitness landscapes by directed evolution. *Nat. Rev. Mol. Cell Biol.* **10,** 866–876 (2009).

32. Shaner, N. C. *et al.* Improved monomeric red, orange and yellow fluorescent proteins derived from *Discosoma* sp. red fluorescent protein. *Nat. Biotechnol.* **22,** 1567–1572 (2004).

Supplementary Information is available in the online version of the paper.

Acknowledgements We thank F. S. Foster, D. Maresca, A. Mukherjee, M. Din, T. Danino, J. Willmann and S. K. Mazmanian for discussions, and A. McDowall for assistance with electron microscopy. This research was supported by the National Institutes of Health grant R01-EB018975, the Canadian Institute of Health Research grant MOP 136842 and the Pew Scholarship in the Biomedical Sciences. A.L. is supported by the NSF graduate research fellowship (award 1144469) and the Biotechnology Leaders Program. A.F. is supported by the NSERC graduate fellowship. S.P.N. was supported by the Caltech Summer Undergraduate Research Fellowship. Research in the Shapiro laboratory is also supported by the Heritage Medical Research Institute, the Burroughs Wellcome Career Award at the Scientific Interface and the David and Lucile Packard Fellowship for Science and Engineering.

Author Contributions R.W.B. and M.G.S. conceived and designed the study. R.W.B., A.L., A.L.-G., A.F. and S.P.N. prepared genetic constructs in *E. coli*. R.W.B., A.L., A.L.-G., S.P.N. and A.F. conducted *in vitro* ultrasound experiments. A.L.-G. and R.W.B. performed *in vivo* ultrasound experiments. A.L., A.F. and A.L.-G. conducted metabolic burden experiments in Nissle 1917 cells. R.W.B. and S.R.K. prepared genetic constructs in *S. typhimurium*. R.W.B. and A.L. obtained TEM images. R.W.B., A.L.-G. and M.G.S. analysed ultrasound data. R.W.B. and M.G.S. wrote the manuscript with input from all authors. M.G.S. supervised the research.

Author Information Reprints and permissions information is available at www.nature.com/reprints. The authors declare no competing financial interests. Readers are welcome to comment on the online version of the paper. Publisher's note: Springer Nature remains neutral with regard to jurisdictional claims in published maps and institutional affiliations. Correspondence and requests for materials should be addressed to M.G.S. (mikhail@caltech.edu).

Reviewer Information *Nature* thanks C. Caskey, O. Couture, P. Silver and the other anonymous reviewer(s) for their contribution to the peer review of this work.

METHODS

Chemicals. All chemicals were purchased from Sigma Aldrich unless otherwise noted.

Molecular cloning. To construct the plasmid for *E. coli* BL21(A1) expression of ARGs, the gene cluster encoding *B. megaterium* gas vesicle proteins GvpBRNFGLSKJTU was amplified from pNL29 (ref. 19) (gift from M. Cannon) and cloned into pET28a using Gibson assembly. The amplicon included an additional 46 base pairs (bp) upstream of the *gvpB* start codon and 180 bp downstream of the *gvpU* stop codon. To generate hybrid gene clusters, the genes encoding GvpA and GvpC were amplified from *A. flos-aquae* and cloned into pET28-RNFGLSKJTU using Gibson assembly. A control gene encoding the green fluorescent protein (GFP) mNeonGreen[33] was similarly constructed in the pET28 vector. For expression of ARGs in *E. coli* Nissle 1917, the pET28 T7 promoter was replaced by the T5 promoter. For *S. typhimurium* expression, the ARG gene cluster was cloned into pTD103 (gift from J. Hasty). A plasmid encoding the luxCDABE gene cluster from *Photorhabdus luminescens* on the pTD103 backbone was also a gift from J. Hasty.

Bacterial expression. Plasmids encoding ARGs or GFP were transformed into chemically competent *E. coli* BL21(A1) cells (Thermo Fisher Scientific) and grown in 5 ml starter cultures in LB medium with 50 μg ml^{-1} kanamycin, 1% glucose for 16 h at 37 °C. Large-scale cultures in LB medium containing 50 μg ml^{-1} kanamycin and 0.2% glucose were inoculated at a ratio of 1:100 with the starter culture. Cells were grown at 37 °C to $OD_{600nm} = 0.5$, then induced with 0.5% L-arabinose and 0.4 mM IPTG for 22 h at 30 °C. For *E. coli* Nissle 1917 (Ardeypharm GmbH) the same protocol was followed, except constructs were electroporated into the cells and induction was performed at $OD_{600nm} = 0.3$ with 3 μM IPTG (*arg1*) and 3 nM *N*-(β-ketocaproyl)-L-homoserine lactone (AHL) (*lux*). Strain identity of *E. coli* Nissle 1917 cells was confirmed by PCR[34]. For *S. typhimurium* expression, the same protocol was followed, except constructs were electroporated into *S. typhimurium* ELH1301 (gift from J. Hasty) and expression was induced with 3 nM AHL.

Gas vesicle purification and quantification. Collected cells were centrifuged at 350*g* in 50 ml conical tubes for 4 h with a liquid height <10 cm to prevent collapse of gas vesicles by hydrostatic pressure. For ARG variants that produce a buoyant band of cells, the middle layer between the buoyant cells and the sedimented cells was removed and discarded. For ARG variants that do not produce a buoyant band, the supernatant was discarded. The remaining cells were resuspended in 8 ml SoluLyse-Tris (L200500 Genlantis) per 100 ml culture and 250 μl ml^{-1} lysozyme, and incubated for 1 h at 4 °C with rotation. Subsequently, 10 μl ml^{-1} DNaseI was added to the lysate and incubated for 10 min at 25 °C. The lysate was transferred to 2 ml tubes and centrifuged for 2 h at 400*g* at 8 °C. The subnatant was removed with a 21.5-gauge needle, and the supernatant containing the gas vesicles was transferred to a clean tube. PBS was added to the gas vesicles in a threefold volume excess and centrifugation, removal of subnatant and PBS dilution was repeated three times. Purified gas vesicles were quantified using the Micro BCA Protein Assay Kit (Thermo Fisher Scientific). Gas vesicles were collapsed with hydrostatic pressure before quantification. Bovine serum albumin was used to generate the standard curve. Absorbance measurements were taken on a Spectramax M5 spectrophotometer (Molecular Devices).

TEM sample preparation and imaging. Cells expressing ARGs, or purified gas vesicles, were exchanged into water or 10 mM HEPES pH 8.0 with 150 mM NaCl, respectively, via three rounds of buoyancy purification and buffer exchange as described above. Samples were deposited on Formvar/carbon 200 mesh grids (Ted Pella) that were rendered hydrophilic by glow discharging (Emitek K100X). For purified gas vesicles, 2% uranyl acetate was added for staining. The samples were then imaged on a FEI Tecnai T12 transmission electron microscope equipped with a Gatan Ultrascan CCD. Images were processed with Fiji[35].

Hydrostatic collapse pressure measurements. Cells expressing ARGs, or purified gas vesicles, were diluted to $OD_{600nm} = 1.0$ in PBS and 0.4 ml was loaded into an absorption cell (176.700-QS, Hellma GmbH). A single valve pressure controller (PC series, Alicat Scientific), supplied by a 1.5-MPa nitrogen gas source, applied hydrostatic pressure in the cell, while a microspectrometer (STS-VIS, Ocean Optics) measured the optical density of the sample at 500 nm. OD_{500nm} was measured from 0 to 1.2 MPa gauge pressure with a 10-kPa step size and a 7-s equilibration period at each pressure.

***In vitro* ultrasound imaging.** Phantoms for imaging were prepared by melting 1% (w/v) agarose in PBS and casting wells using a custom 3D-printed template. Cells at 2× the final concentration were mixed in a 1:1 ratio with molten agarose (at 50 °C) and immediately loaded into the phantom. The concentration of cells was determined before loading by measuring their OD_{600nm} after exposure to 1.2 MPa hydrostatic pressure to eliminate any contribution to light scattering from gas vesicles. The optical density was then converted into cells per ml using the relationship 1 OD = 8×10^8 cells ml^{-1} (https://www.genomics.agilent.com/biocalculators/calcODBacterial.jsp). Cell samples collected at early time points following induction, which had an optical density insufficient for loading, were first concentrated using centrifugation at 350*g*. Ultrasound imaging was performed using a Verasonics Vantage programmable ultrasound scanning system and L22-14v 128-element linear array transducer (Verasonics). The transducer was mounted on a computer-controlled 3D translatable stage (Velmex). Image acquisition was performed using conventional B-mode imaging using a 128-ray-lines protocol with a synthetic aperture to form a focused excitation beam. The transmit waveform was set to a frequency of 19 MHz, 67% intra-pulse duty cycle, and a one-cycle pulse. Samples were positioned 6 mm from the transducer face, which is the elevation focus of the L22-14v transducer, coupled through a layer of PBS. The transmit beam was also digitally focused at 6 mm. For imaging, the transmit voltage was 2 V and the *f*-number was 3, resulting in a peak positive pressure of 0.4 MPa. Backscattered ultrasound signals were filtered with a 7-MHz bandpass filter centred at 19 Mhz. Signals backscattered from four transmit events were summed before image processing. Pixel gain was set to 3 and persistence to 90.

For gas vesicle collapse using the L22-14 array, we set the *f*-number to 0.2 (thereby ensuring that all transducer elements were active) and scanned the transmit focus from 3 mm to 9 mm. During the 10-s collapse scan, single-cycle pulses were applied using a ray-lines protocol at 19 MHz with a frame rate of 12 frames per second. To measure gas vesicle collapse in ARG-expressing cells as a function of acoustic pressure, images were acquired as described above at a peak positive pressure of 0.4 MPa after sequentially exposing the samples to collapse pulses of increasing amplitude, with pressures that varied from 0.55 MPa to 4.7 MPa. To achieve complete collapse, we applied the maximal pressure of 4.7 MPa. Collapse data were fitted with a Boltzmann sigmoid function to facilitate visualization of collapse curves. This function is of the form $f(p) = \left(1 + e^{\frac{p-p_c}{s}}\right)^{-1}$ where p is the pressure, and p_c and s are fitted parameters representing the collapse midpoint and slope, respectively. For spectral unmixing, the two collapse pressures applied were 2.7 MPa and 4.7 MPa. Transducer output pressures were measured in a degassed water tank using a fibre-optic hydrophone (Precision Acoustics).

Plate-based induction and optical imaging. ARG and GFP constructs were transformed as described above, and the transformation mix after recovery was plated on two-layer LB-Agar plates. The underlayer contained 50 μg ml^{-1} kanamycin, 1.0% L-arabinose, and 0.8 mM IPTG. The overlayer contained 50 μg ml^{-1} kanamycin and 0.4% glucose. The overlayer was poured 30 min before plating, and each layer was 4 mm thick. Plates with transformants were incubated at 30 °C for 20 h and then imaged for white light scattering and green fluorescence using a Chemidoc MP instrument (Bio-Rad).

Cell growth, viability and microcin production assays. *E. coli* Nissle 1917 cells were transformed by electroporation with pET28 plasmids containing either the *arg1* or *lux* gene cluster under the T5 promoter. Transformed cells were grown in 5 ml starter cultures in LB medium containing 50 μg ml^{-1} kanamycin, 1% glucose for 16 h at 37 °C. The overnight cultures were diluted 1:100 in 50 ml of LB medium containing 50 μg ml^{-1} kanamycin and 0.2% glucose. Cultures were grown at 30 °C to $OD_{600nm} \approx 0.2–0.3$ and induced with 3 μM IPTG (+IPTG), or left uninduced (−IPTG). Both induced and uninduced cultures were allowed to grow for 22 h at 30 °C. For time point optical density measurements, 1 ml of the culture was taken out and measured. For plating after 22 h of growth, the cultures were diluted to a uniform OD_{600nm} of 0.2, before further serial dilution by a factor of 2×10^4 in LB supplemented with 50 μg ml^{-1} kanamycin and 0.2% glucose. 100 μl of the final dilutions was plated on two-layer LB agar plates using a cell spreader. The underlayer of the plates contained 50 μg ml^{-1} kanamycin and 9 μM IPTG. The overlayer contained 50 μg ml^{-1} kanamycin and 0.4% glucose. The overlayer was poured 30 min before plating, and each layer was 3 mm thick. Cells uniformly spread on the two-layer plates were allowed to grow at 30 °C for 21 h. Colonies were then imaged for light scattering using the Chemidoc MP instrument under white light transillumination and 605 ± 50 nm receive filter, and both opaque (gas vesicle-producing) and clear colonies were counted to determine total colony forming units per millilitre and the gas vesicle-expressing fraction. Plates had a minimum of 82 and a maximum of 475 total colonies, enabling manual counting.

To assay microcin production, *E. coli* Nissle 1917 cells containing *arg1* or *lux* were cultured as described above and spotted on microcin assay plates containing *E. coli* K-12 H5316 cells (gift from K. Hantke). Wild-type H5316 were grown in 5 ml LB medium, and H5316 cells transformed with pET plasmid containing mWasabi and KanR under a T5 promoter (H5316* cells) were grown in 5 ml LB medium containing 50 μg ml^{-1} kanamycin and 1% glucose for 16 h at 37 °C. Two-layer LB plates were used to assay the growth inhibition of H5316 cells by microcin peptides produced by Nissle 1917 cells. Plates used to assay with wild-type H5316 cells contained 20 ml of 1% LB agar at the bottom, and the top layer contained 2×10^7 H5316 cells in 20 ml of 0.3% LB agar. Plates using H5316* cells contained 20 ml of 1% LB agar with 50 μg ml^{-1} kanamycin, 50 μM desferal, and 3 μM IPTG, and the top layer contained 2×10^7 H5316* cells in 20 ml of 0.3% LB agar with 50 μg ml^{-1} kanamycin, 50 μM desferal, and 3 μM IPTG. Nissle cells containing

arg1 or *lux* genes were cultured at 30 °C for 22 h with or without 3 μM IPTG. Nissle cells with *arg1* were exposed to 1 MPa of hydrostatic pressure to facilitate the removal of kanamycin by centrifugation before spotting on H5316 plates. Nissle cells containing *arg1* and *lux* induced and uninduced with IPTG, as well as H5316* cells, were washed 3× in PBS by pelleting and adjusted to $OD_{600nm} = 1$ in LB. All cells were spotted in 2-μl volume on 5-mm sterile filter paper (Bel-Art Products), placed on the microcin assay plates. Unsupplemented LB and 100 mg ml^{-1} ampicillin (2 μl each) were similarly spotted as controls. After 17 h at 37 °C, the plates were imaged with the Chemidoc MP instrument with blue transillumination, and unfiltered light was collected to form an image. Images shown are representative of four experiments each.

Colony ultrasound. ARG and GFP constructs were transformed into BL21(A1) one-shot competent cells (Thermo Fisher Scientific) and plated onto LB agar two-layer inducer plates as described above. Plates were grown at 37 °C for 14h. The colonies were immobilized by depositing a 4 mm layer of 0.5% agarose–PBS gently onto the plate surface. Ultrasound imaging was performed using a L11-4v128-element linear array transducer (Verasonics) to obtain a larger field of view. The transducer was mounted on a computer-controlled 3D translatable stage (Velmex). Image acquisition was performed using conventional B-mode imaging using a 128-ray-lines protocol with a synthetic aperture to form a focused excitation beam. The transmit waveform was set to a frequency of 6.25 MHz, 67% intra-pulse duty cycle, and a four-cycle pulse. Colonies were positioned 20 mm from the transducer face, which is the elevation focus of the L11-4v transducer, coupled through a layer of PBS. The transmit beam was also digitally focused at 20 mm. For imaging, the transmit power was 2 V and the *f*-number was 3, resulting in a peak positive pressure of 0.61 MPa. To measure gas vesicle collapse in bacterial colonies as a function of acoustic pressure, images were acquired as described above at a peak positive pressure of 0.61 MPa after sequentially exposing the samples to collapse pulses at 6.25 MHz, with increasing amplitude from 0.61 MPa to 5.95 MPa. Pixel gain in the images was set to 0.1 and persistence to 20. Cross-sectional images of the plate (perpendicular to the plate surface) were acquired at spatial intervals of 250 μm using computer-controlled steps. The cross-sectional images were processed in MATLAB to form 2D images of the plate surface. First, the cross-sectional images were stacked to produce a 3D-volumetric reconstruction of the plate. We then summed the signals in a 2-mm slice of the volume parallel to and centred on the bacterial growth surface after thresholding to eliminate background, forming a 2D projection image of the plate. After ultrasound imaging, image processing, and acoustic phenotype prediction, the colonies were picked using 10-μl sterile pipette tips. Each colony was used to inoculate a 5-ml LB culture containing 50 μg ml^{-1} kanamycin culture. DNA was extracted from the cultures by mini-prep (PureYield, Promega) and sequenced to determine whether the plasmid contained GFP, *arg1* or *arg2*.

***In vivo* ultrasound and bioluminescence imaging.** All *in vivo* experiments were performed on BALB/c or SCID nude female mice, aged 14–15 weeks, under a protocol approved by the Institutional Animal Care and Use Committee of the California Institute of Technology. No randomization or blinding were necessary in this study. Ultrasound imaging was performed as follows. Mice were anaesthetized with 1–2% isoflurane, maintained at 37 °C on a heating pad, depilated over the imaged region, and imaged using an L22-14v transducer with the pulse sequence described above. For imaging of *E. coli* in the gastrointestinal tract, BALB/c mice were placed in a supine position, with the ultrasound transducer positioned on the lower abdomen, transverse to the colon. Anatomical landmarks including the bladder were used to identify the position of the colon. Prior to imaging, buoyancy-enriched *E. coli* Nissle 1917 expressing *arg1* or *lux* were mixed in a 1:1 ratio with 42 °C 4% agarose–PBS for a final bacterial concentration of 10^9 cells ml^{-1}. An 8-gauge needle was filled with the mixture of agarose and bacteria expressing either *arg1* or *lux*. Before it solidified, a 14-gauge needle was placed inside the 8-gauge needle to form a hollow lumen within the gel. After the agarose–bacteria mixture solidified at room temperature for 10 min, the 14-gauge needle was removed. The hollow lumen was then filled with the agarose–bacteria mixture expressing the other imaging reporter (*arg1* or *lux*). After it solidified, the complete cylindrical agarose gel was injected into the colon of the mouse with a PBS back-filled syringe. The same procedure was used with *E. coli* BL21 cells, except with the entire gel homogeneously composed of either *arg2*- or GFP-expressing cells. Introduction of gel into the colon is a common preparatory protocol for gastrointestinal ultrasound[36,37].

For imaging of *S. typhimurium* in tumours, we formed hind-flank ovarian tumour xenografts in SCID nude mice via subcutaneous injection of 5×10^7 OVCAR8 cells (provided by the National Cancer Institute tumour repository with certificate of authentication) with Matrigel. After tumours grew to dimensions larger than approximately 6 mm (14 weeks), they were injected with *arg1*-expressing *S. typhimurium*, (50 μl, 3.2×10^9 cells ml^{-1}). The tumours were then imaged with ultrasound, with anaesthetized mice in a prone position (homeostasis and imaging parameters as described above). Our animal protocol specified that animals with total tumour volume exceeding 2 cm^3, or showing signs of distress as assessed by the veterinary team, be euthanized.

For luminescence imaging, mice were anaesthetized with 100 mg kg^{-1} ketamine and 10 mg kg^{-1} xylazine and imaged using a Bio-Rad ChemiDoc MP imager without illumination, no emission filter, and an integration time of 5 min. The image was thresholded and rendered in ImageJ, and superimposed on a bright-field image of the mouse using GIMP.

Image processing. MATLAB was used to process ultrasound images. Regions of interest (ROIs) were defined to capture the ultrasound signal from the phantom well, colon, or tumour region. All *in vitro* phantom experiments had the same ROI dimensions. For *in vivo* experiments ROIs were selected consistently to exclude edge effects from the colon wall or skin. Mean pixel intensity was calculated from each ROI, and pressure-sensitive ultrasound intensity was calculated by subtracting the mean pixel intensity of the collapsed image from the mean pixel intensity of the intact image. Images were pseudo-coloured, with maximum and minimum levels adjusted for maximal contrast as indicated in accompanying colour bars.

For the multiplexed imaging of *arg1* and *arg2*, acoustic spectral unmixing was performed as previously described[20]. In brief, a spatial averaging filter (kernel size 30 × 30 pixels or 750 × 750 μm) was applied to the three acquired images (before collapse, after collapse with 2.7 MPa and after collapse with 4.7 MPa) to reduce noise. Then, pixel-wise differences between the first and second image, and between the second and third image were calculated, and multiplied by the inverse of the collapse matrix, α, representing the expected fractional collapse of each ARG type at each pressure ($\alpha = (0.7921, 0.5718; 0.2079, 0.4282)$), to produce the unmixed pixel intensities corresponding to the contributions from *arg2* and *arg1*.

Statistical analysis. For statistical significance testing, we used two-sided heteroscedastic *t*-tests with a significance level of type I error set at 0.05 for rejecting the null hypothesis. Sample sizes for all experiments, including animal experiments, were chosen on the basis of preliminary experiments to be adequate for statistical analysis.

Code availability. MATLAB code is available from the corresponding author upon reasonable request.

Data and code availability. *arg1* and *arg2* plasmid sequences are included in Supplementary Information, and plasmids will be available from Addgene. All other materials are available from the corresponding author upon reasonable request.

33. Shaner, N. C. *et al.* A bright monomeric green fluorescent protein derived from *Branchiostoma lanceolatum*. *Nat. Methods* **10,** 407–409 (2013).
34. Blum-Oehler, G. *et al.* Development of strain-specific PCR reactions for the detection of the probiotic *Escherichia coli* strain Nissle 1917 in fecal samples. *Res. Microbiol.* **154,** 59–66 (2003).
35. Schindelin, J. *et al.* Fiji: an open-source platform for biological-image analysis. *Nat. Methods* **9,** 676–682 (2012).
36. Wang, H. *et al.* Molecular imaging of inflammation in inflammatory bowel disease with a clinically translatable dual-selectin-targeted US contrast agent: comparison with FDG PET/CT in a mouse model. *Radiology* **267,** 818–829 (2013).
37. Freeling, J. L. & Rezvani, K. Assessment of murine colorectal cancer by micro-ultrasound using three dimensional reconstruction and non-linear contrast imaging. *Mol. Ther. Methods Clin. Dev.* **3,** 16070 (2016).

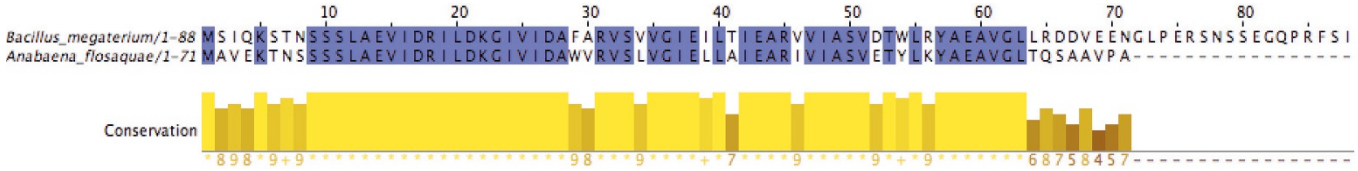

Extended Data Figure 1 | Sequence homology of GvpA/B. Amino acid sequence alignment of the primary gas vesicle structural protein GvpB from *B. megaterium* (the GvpA analogue in this species) and GvpA from *A. flos-aquae*.

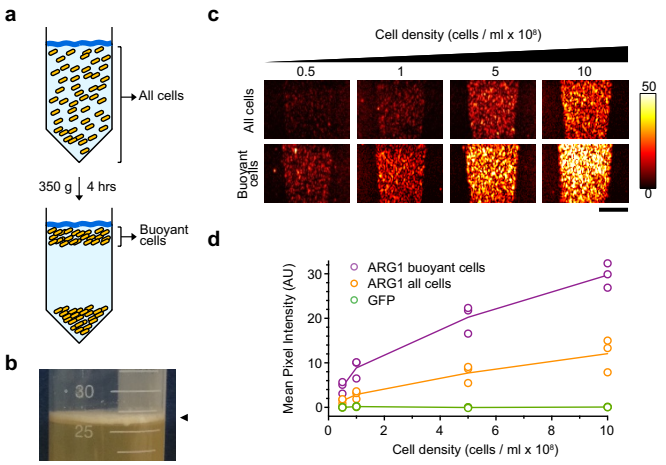

Extended Data Figure 2 | Ultrasound contrast from buoyancy-enriched cells. a, Diagram of centrifugation-assisted enrichment of buoyant cells. **b**, Image of *arg1 E. coli* culture 22 h after induction and 4 h of centrifugation at 350*g*, showing the presence of buoyant cells. Arrowhead points to the meniscus layer containing buoyant cells. Experiment repeated three times with similar results. **c**, Ultrasound images of *E. coli* expressing *arg1* at various cellular concentrations, with and without buoyancy enrichment. Experiment was repeated three times with similar results. **d**, Ultrasound contrast from *E. coli* expressing *arg1*, with and without buoyancy enrichment, and GFP at various cell densities. Data are from three biological replicates; lines represent the mean.

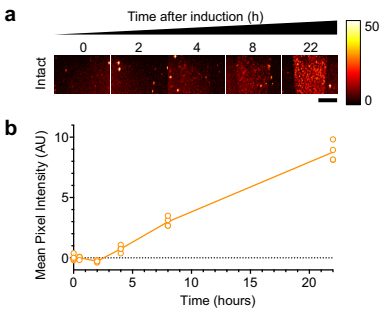

Extended Data Figure 3 | Time course of acoustic reporter gene contrast after induction. a, Ultrasound images of *arg1*-expressing *E. coli* at various times after induction with IPTG. Experiment repeated four times with similar results. **b**, Ultrasound contrast at each time point. Data are from four biological replicates; line represents the mean. Cell concentration, 5×10^8 cells ml^{-1}. Scale bar, 2 mm.

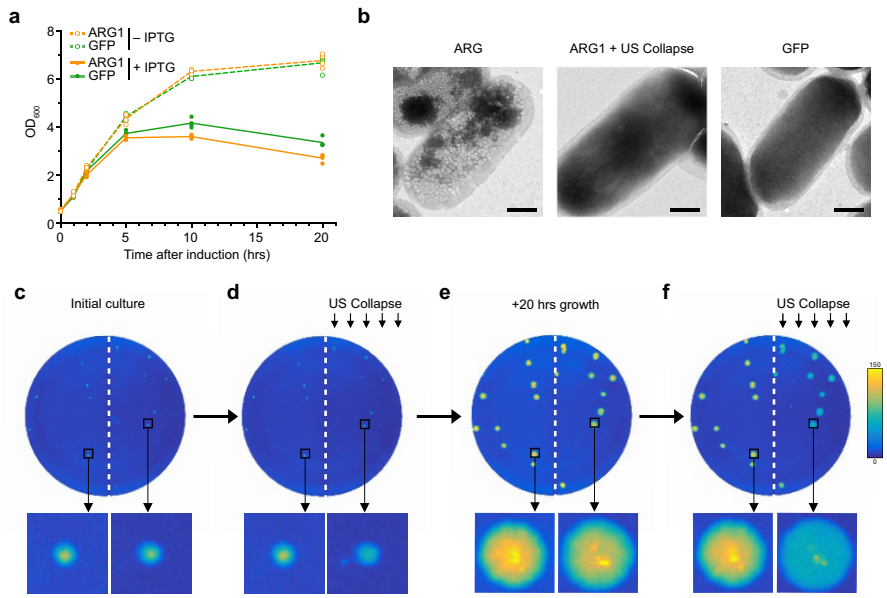

Extended Data Figure 4 | Acoustic reporter gene expression and ultrasound imaging does not affect cell viability. a, Growth curves of *E. coli* containing the *arg1* or GFP expression plasmid, with or without induction using 0.4 mM IPTG. Data are from three biological replicates per sample; lines represent the mean. **b**, Representative TEM images of whole *E. coli* cells expressing *arg1* with and without exposure to acoustic collapse pulses, and *E. coli* cells expressing GFP. Images were acquired from three biologically independent samples for *arg1*, two for *arg1* with ultrasound collapse and one for GFP (more than 50 cells imaged per sample) with similar results. **c**, Dark-field optical image of agar plate containing colonies of *E. coli* expressing *arg1* 14 h after seeding. **d**, Image of the same plate after the right half of the plate was insonated with high-pressure ultrasound. **e**, Image of the same plate 20 h after insonation. **f**, Image after the right half of the plate in **e** was insonated with high-pressure ultrasound. Zoomed in images of representative colonies shown below each plate image. Scale bars, 500 nm. Experiment was repeated three times with similar results.

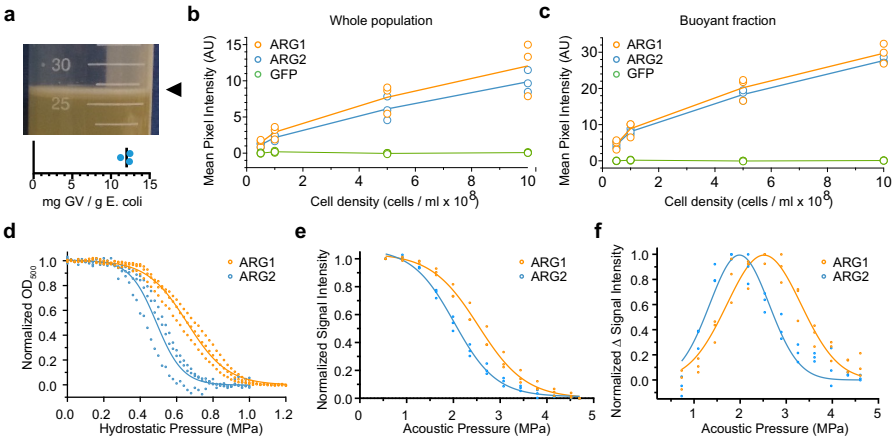

Extended Data Figure 5 | Multiplexed imaging of genetically engineered reporter variants. a, Image of *arg2 E. coli* culture 22 h after induction showing the presence of buoyant cells (top). Experiment repeated three times with similar results. Mass fraction of gas vesicles produced 22 h after induction (bottom). Line represents the mean. **b**, Ultrasound contrast from the whole population of cells expressing *arg1*, *arg2* or GFP. Lines represent the mean. **c**, Ultrasound contrast from the buoyancy-enriched population of cells expressing *arg1*, *arg2* or GFP. Lines represent the mean. **d**, Normalized optical density (representing the intact fraction) of gas vesicles isolated from *E. coli* expressing *arg1* or *arg2* as a function of applied hydrostatic pressure. **e**, Normalized ultrasound intensity as a function of peak positive pressure from 0.6 to 4.7 MPa for *E. coli* expressing *arg1* or *arg2*. **f**, Acoustic collapse spectra derived by differentiating the data and curves in **e** with respect to applied pressure. **a**–**f**, Data are from three biological replicates per sample. **d**–**f**, Curves represent fits of the data using the Boltzmann sigmoid function to assist visualization.

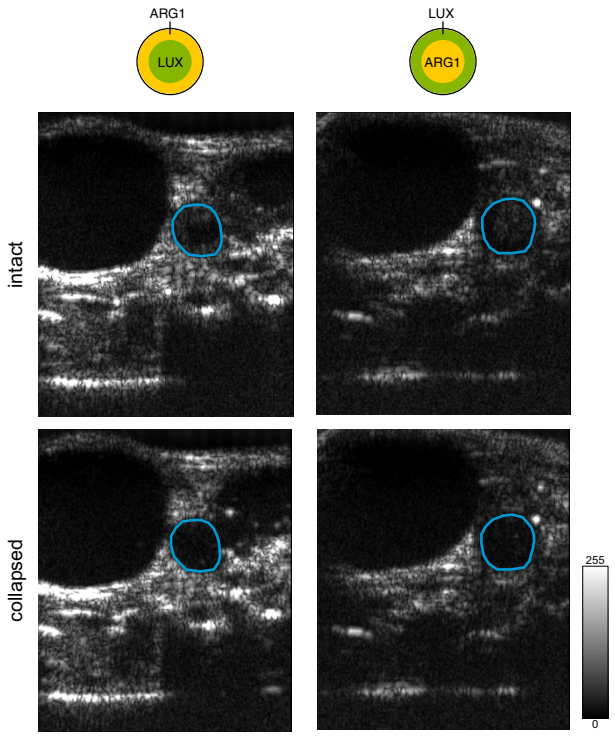

Extended Data Figure 6 | Anatomical ultrasound images of acoustic bacteria in the gastrointestinal tract. Raw images underlying the difference maps shown in Fig. 4e, g. The cyan outline identifies the colon region of interest for difference processing. This experiment was repeated three times with similar results.

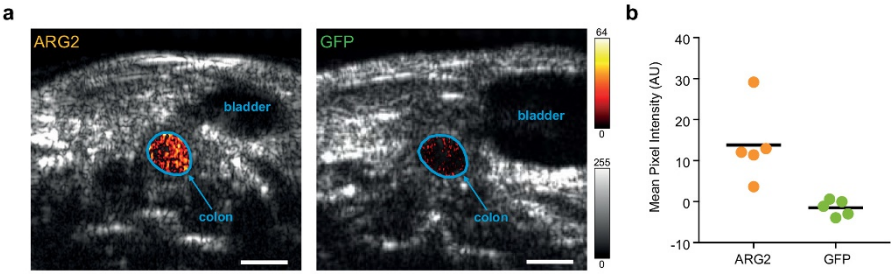

Extended Data Figure 7 | Ultrasound imaging of ARG-expressing cells in the mouse colon. a, Transverse ultrasound images of mice whose colon contains BL21 *E. coli* expressing either *arg2* or GFP at a final concentration of 10^9 cells ml^{-1}. A difference heat map of ultrasound contrast within the colon region of interest before and after acoustic collapse is overlaid on a grayscale anatomical image. **b**, Signal intensity in mice with *E. coli* expressing either *arg2* or GFP. Data are from 5 biological replicates per sample. *P* value = 0.02 using two-sided heteroscedastic *t*-test. Scale bar, 2 mm.

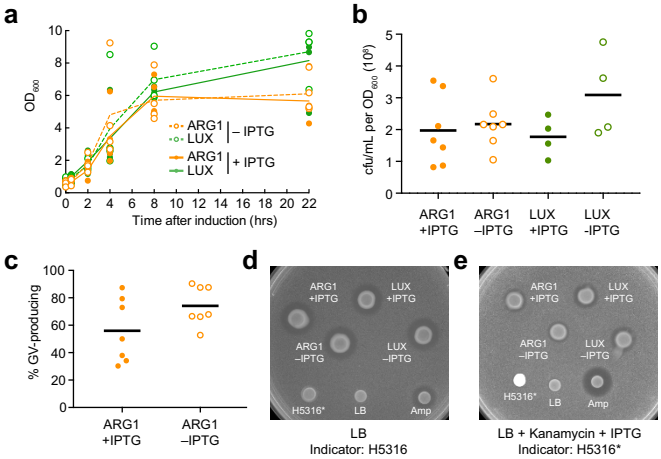

Extended Data Figure 8 | Effect of *arg1* and *lux* expression on ECN cell growth, viability and microcin release. a, Optical density at 600 nm measured from 0 to 22 h after induction with 3 μM IPTG, or without induction, in ECN cells transformed with *arg1* or *lux*. Data are from four biological replicates per time point, lines represent the mean. For comparisons between induced *arg1* and induced *lux* values at 22 h $P = 0.12$. For comparisons between uninduced *arg1* and uninduced *lux* at 22 h $P = 0.04$. For comparisons at all other time points $P > 0.14$. **b**, Colony-forming units (cfu) per millilitre culture per OD_{600nm} after 22 h of induction with 3 μM IPTG, or uninduced growth, of ECN cells transformed with *arg1* or *lux*. $P \geq 0.22$. Data are from 7 biological replicates for *arg1* samples and four biological replicates for *lux* samples. Lines represent the mean. **c**, Fraction of opaque, gas vesicle-producing colonies produced by plating *arg1*-transformed ECN cells 22 h after induction with 3 μM IPTG, or uninduced growth. Cells were plated on dual-layer IPTG induction plates, allowed to grow overnight at 30 °C, and imaged as in (Extended Data Fig. 4c–f, $P = 0.12$. data are from seven biological replicates, lines represent the mean. **d**, Microcin release assay using a uniform layer of the indicator strain *E. coli* K12 H5316 in soft agar, after 17-h incubation with filters containing microcin sources and controls, as indicated. ECN cells transformed with *arg1* or *lux* were induced for 22 h with 3 μM IPTG, or grown without induction, before spotting. H5316* indicates H5316 cells transformed with mWasabi and cultured for 22 h as with ECN cells. All cells were washed before spotting to remove antibiotic. Experiment was performed four times with similar results. Amp, 100 mg ml^{-1} ampicillin; LB, LB medium. **e**, As in **d**, but with the indicator strain comprising H5316* cells and the agar containing 50 μg ml^{-1} kanamycin, 3 μM IPTG and 50 μM desferal, to show that microcin release also occurs during transgene expression. Note that the H5316* spot appears bright because the plate image is acquired with blue-light transillumination, resulting in mWasabi fluorescence. Experiment was performed four times with similar results. All *P* values were calculated using a two-sided heteroscedastic *t*-test.

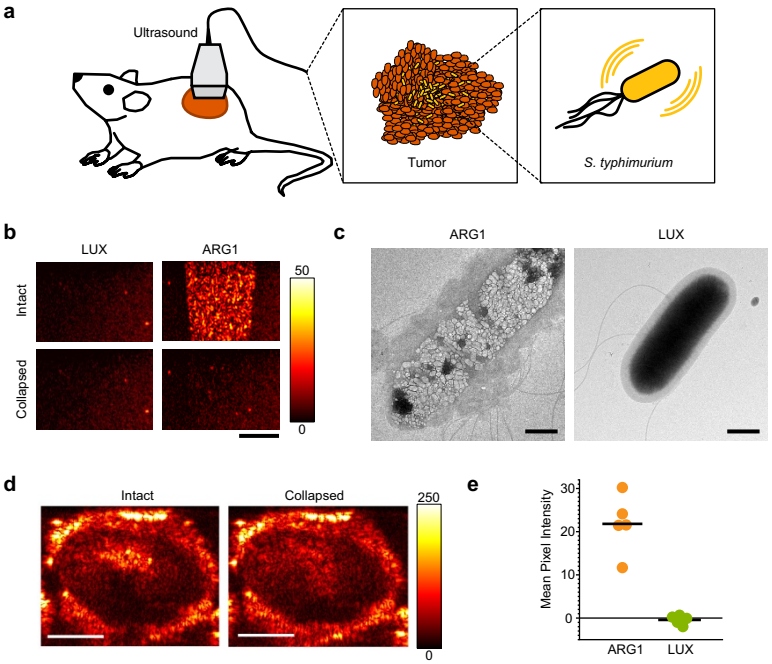

Extended Data Figure 9 | Ultrasound imaging of *S. typhimurium* in tumour xenografts. a, Diagram of tumour imaging experiment. *S. typhimurium* expressing *arg1* were introduced into the tumours of mice and imaged with ultrasound. **b**, Ultrasound images of a gel phantom containing *S. typhimurium* expressing *arg1* or the *lux* operon. Cell concentration is 10^9 cells ml^{-1}. Experiment repeated three times with similar results. **c**, TEM images of whole *S. typhimurium* cells expressing *arg1* with and without exposure to acoustic collapse pulses. At least 20 cellular images were acquired for each sample type (from one biological preparation each) with similar results. **d**, Ultrasound images of mouse OVCAR8 tumours injected with 50 µl of 3.2×10^9 cells ml^{-1} *arg1*-expressing *S. typhimurium*, before and after acoustic collapse. Experiment repeated five times with similar results. **e**, Collapse-sensitive ultrasound contrast in tumours injected with *arg1*-expressing or *lux*-expressing cells. Data are from five animals, line represents the mean. $P = 0.002$ using a two-sided heteroscedastic *t*-test. Scale bars, 2 mm (**b**), 500 nm (**c**) and 2.5 mm (**d**).

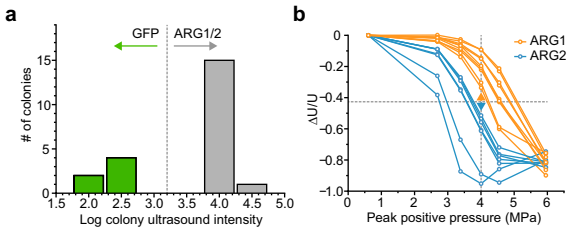

Extended Data Figure 10 | High-throughput screening of acoustic phenotypes. a, Ultrasound intensity histogram of 22 randomly picked colonies. Colonies with low contrast were predicted to contain the gene encoding GFP and those with high contrast to contain genes encoding *arg1* or *arg2* genes. **b**, Normalized change in ultrasound intensity (U) for each of the 15 *arg1* or *arg2* colonies after insonation at increasing pressures. At 4 MPa, colonies with signal above the indicated threshold were predicted to be *arg1* and below to be *arg2*. This experiment was performed once; each colony was treated as a biological replicate.

nature research

Corresponding author(s): Mikhail G. Shapiro

☐ Initial submission ☐ Revised version ☒ Final submission

Life Sciences Reporting Summary

Nature Research wishes to improve the reproducibility of the work that we publish. This form is intended for publication with all accepted life science papers and provides structure for consistency and transparency in reporting. Every life science submission will use this form; some list items might not apply to an individual manuscript, but all fields must be completed for clarity.

For further information on the points included in this form, see Reporting Life Sciences Research. For further information on Nature Research policies, including our data availability policy, see Authors & Referees and the Editorial Policy Checklist.

Experimental design

1. Sample size

Describe how sample size was determined.

Sample sizes for all experiments, including animal experiments, were chosen on the basis of preliminary experiments to be adequate for statistical analysis.

2. Data exclusions

Describe any data exclusions.

n/a

3. Replication

Describe whether the experimental findings were reliably reproduced.

Stated in figure captions.

4. Randomization

Describe how samples/organisms/participants were allocated into experimental groups.

No randomization was necessary in this study.

5. Blinding

Describe whether the investigators were blinded to group allocation during data collection and/or analysis.

No blinding was necessary in this study.

Note: all studies involving animals and/or human research participants must disclose whether blinding and randomization were used.

6. Statistical parameters

For all figures and tables that use statistical methods, confirm that the following items are present in relevant figure legends (or in the Methods section if additional space is needed).

n/a	Confirmed
☐	☒ The exact sample size (*n*) for each experimental group/condition, given as a discrete number and unit of measurement (animals, litters, cultures, etc.)
☐	☒ A description of how samples were collected, noting whether measurements were taken from distinct samples or whether the same sample was measured repeatedly
☐	☒ A statement indicating how many times each experiment was replicated
☐	☒ The statistical test(s) used and whether they are one- or two-sided (note: only common tests should be described solely by name; more complex techniques should be described in the Methods section)
☐	☒ A description of any assumptions or corrections, such as an adjustment for multiple comparisons
☐	☒ The test results (e.g. *P* values) given as exact values whenever possible and with confidence intervals noted
☐	☒ A clear description of statistics including central tendency (e.g. median, mean) and variation (e.g. standard deviation, interquartile range)
☒	☐ Clearly defined error bars

See the web collection on statistics for biologists for further resources and guidance.

Software

Policy information about availability of computer code

7. Software

Describe the software used to analyze the data in this study.	MATLAB used for data and image analysis. MATLAB, Excel and Prism used for fitting and plotting.

For manuscripts utilizing custom algorithms or software that are central to the paper but not yet described in the published literature, software must be made available to editors and reviewers upon request. We strongly encourage code deposition in a community repository (e.g. GitHub). *Nature Methods* guidance for providing algorithms and software for publication provides further information on this topic.

Materials and reagents

Policy information about availability of materials

8. Materials availability

Indicate whether there are restrictions on availability of unique materials or if these materials are only available for distribution by a for-profit company.	All materials and data available on reasonable request. ARG1 and ARG2 plasmids will be deposited to Addgene.

9. Antibodies

Describe the antibodies used and how they were validated for use in the system under study (i.e. assay and species).	n/a

10. Eukaryotic cell lines

a. State the source of each eukaryotic cell line used.	n/a
b. Describe the method of cell line authentication used.	n/a
c. Report whether the cell lines were tested for mycoplasma contamination.	n/a
d. If any of the cell lines used are listed in the database of commonly misidentified cell lines maintained by ICLAC, provide a scientific rationale for their use.	n/a

Animals and human research participants

Policy information about studies involving animals; when reporting animal research, follow the ARRIVE guidelines

11. Description of research animals

Provide details on animals and/or animal-derived materials used in the study.	Information included in the "In vivo ultrasound and bioluminescence imaging" section of the Methods

Policy information about studies involving human research participants

12. Description of human research participants

Describe the covariate-relevant population characteristics of the human research participants.	n/a